DE GRUYTER
OPEN

Journal of ELECTRICAL ENGINEERING, VOL 67 (2016), NO4, 292–298

STATISTICAL PROPERTIES OF REAL–TIME AMPLITUDE ESTIMATE OF HARMONICS AFFECTED BY FREQUENCY INSTABILITY

Diego Bellan — Sergio A. Pignari *

This work deals with the statistical characterization of real-time digital measurement of the amplitude of harmonics affected by frequency instability. In fact, in modern power systems both the presence of harmonics and frequency instability are well-known and widespread phenomena mainly due to nonlinear loads and distributed generation, respectively. As a result, real-time monitoring of voltage/current frequency spectra is of paramount importance as far as power quality issues are addressed. Within this framework, a key point is that in many cases real-time continuous monitoring prevents the application of sophisticated algorithms to extract all the information from the digitized waveforms because of the required computational burden. In those cases only simple evaluations such as peak search of discrete Fourier transform are implemented. It is well known, however, that a slight change in waveform frequency results in lack of sampling synchronism and uncertainty in amplitude estimate. Of course the impact of this phenomenon increases with the order of the harmonic to be measured. In this paper an approximate analytical approach is proposed in order to describe the statistical properties of the measured magnitude of harmonics affected by frequency instability. By providing a simplified description of the frequency behavior of the windows used against spectral leakage, analytical expressions for mean value, variance, cumulative distribution function, and probability density function of the measured harmonics magnitude are derived in closed form as functions of waveform frequency treated as a random variable.

K e y w o r d s: digital measurements, discrete Fourier transform, frequency-domain analysis, frequency instability, harmonics, statistical analysis

1 INTRODUCTION

Modern electrical power systems are characterized by increasing complexity mainly due to the so-called distributed generation (DG) and to the widespread use of nonlinear loads. In particular, the use of time-varying nonlinear loads (*eg*, [1]) requires a continuous real-time monitoring of the harmonic content in the voltage/current waveforms spectra for power quality purposes [2]. It is well-known, however, that one of the drawbacks of DG is frequency instability/inaccuracy of the generated waveforms [3–5]. Therefore, as the main objective of this paper, it is of paramount importance to investigate the effect of frequency instability on the harmonics measurements performed by digital techniques based on analog-to-digital (A/D) conversion of the waveforms and the discrete Fourier transform (DFT) usually evaluated through the fast Fourier transform (FFT).

In the past literature many papers have been devoted to sophisticated algorithms to treat the case of non-coherent sampling (*eg*, see [6, 7]), *ie*, the case of a sampling frequency which is not integer multiple of the frequency of a sine wave component. Such algorithms allow to recover the magnitude of each sine wave component with high accuracy. However, when a continuous real-time monitoring of a wide spectrum is required, implementation of sophisticated algorithms could be not effective due to the required computational burden.

In this paper it is assumed that harmonics monitoring is performed by repeated digitization of waveform windows with given length, *ie*, by A/D conversion of N_S-sample windows consisting of samples taken with a given sampling frequency. Each N_S-sample window is transformed into the frequency domain (*ie*, the DFT) through the FFT, and the peaks at harmonics locations provide the estimated magnitude of each harmonic. Due to frequency instability, it is expected that from one N_S-sample window to another, each harmonic slightly changes its frequency and, as a consequence, the magnitude of the related peak in the DFT changes. By treating each harmonic frequency as a random variable, the harmonic magnitude is a random variable as well, whose statistical properties will be derived in closed form as functions of the frequency distribution and of the specific window used against spectral leakage. In particular, an approximate analytical representation of the frequency behavior of the windows used against spectral leakage will be provided. This approach allows the analytical derivation of mean value, variance, cumulative distribution function, and probability density function of the measured harmonic amplitude as functions of the frequency distribution.

* Department of Electronics, Information and Bioengineering, Politecnico di Milano, Piazza Leonardo da Vinci 32, 20133 Milan, Italy, diego.bellan@polimi.it

DOI: 10.1515/jee-2016-0043, Print (till 2015) ISSN 1335-3632, On-line ISSN 1339-309X

The paper is organized as follows. In Section 2 the statement of the problem is provided. In Section 3 the statistical properties of the measured harmonic amplitude are derived under the assumption of frequency instability spanning less than one frequency bin of the discrete Fourier transform. In Section 4 the approach and results are extended to the case of frequency instability involving more than one DFT frequency bin. Validation through numerical simulations is provided in Section 5. Finally, concluding remarks are discussed in Section 6.

2 PROBLEM STATEMENT

Measurement of power system harmonics can be effectively performed by resorting to digital instrumentation based on A/D conversion of voltage and current waveforms, and time-to-frequency transformation through the DFT (with the efficient FFT algorithm) [6–8]. Thus, harmonics magnitude at each frequency of interest can be readily evaluated by reading the amplitude of the relevant spectral lines.

Two main sources of uncertainty can be identified in the measurement process outlined above. First, the fundamental frequency of voltage/current waveforms is typically affected by random instability. It means that by repeating the measurement process, slightly different values of the waveforms fundamental frequency must be expected. Such frequency instability is of course emphasized for harmonic components. When the DFT is applied, the lack of synchronism between the frequency of the waveform sinusoidal components and the sampling frequency (*ie*, non-coherent sampling) will result in increased uncertainty in the amplitude measurements. The second main source of uncertainty is additive noise. Indeed, voltage/current waveforms are always affected by additive noise which propagates through A/D conversion and DFT transformation, yielding noisy spectral lines. It is expected that the impact of additive noise is larger as the amplitude of the involved harmonic spectral lines decreases. Spectral effects of additive noise have been already investigated in many previous papers [8–12]. Therefore, in this work additive noise will not be considered by assuming that noise effects can be readily included by resorting to previous literature results.

The time-domain voltage waveform is modelled as a sum of N sine waves

$$v(t) = \sqrt{2}\sum_{h=1}^{N} V_h \cos\big(2\pi f_h t + \varphi_h\big), \tag{1}$$

where $f_h = hf_1$. A similar expression holds for the current waveform, therefore in this paper mathematical derivations will be presented for the voltage waveform only.

After A/D conversion of (1) with sampling frequency f_S, and weighted time-windowing (N_S samples in length) against spectral leakage [13], the DFT transform provides the estimates of the complex Fourier coefficients

$$\overline{V}_n = \frac{\sqrt{2}}{N_S \mathrm{NPSG}} \sum_{k=0}^{N_S-1} v[k]w[k]exp\big(-j2\pi kn/N_S\big), \tag{2}$$

where $w[k]$ is the selected time window characterized by the related normalized peak signal gain NPSG (see Tab. 1 where three examples of commonly used windows are reported with the parameters exploited in this paper). The frequency index n is related to the frequency index h in (1) by $n \times \Delta f = f_h$, where $\Delta f = f_S/N_S$ is the DFT frequency resolution. Under non-coherent sampling, the relation $n \times \Delta f = f_h$ is intended as an approximate relation where n is the index such that $n \times \Delta f$ is the discrete frequency closest to f_h.

In the next two sections the statistical properties of $\hat{V}_n = |\overline{V}_n|$ will be derived as functions of the statistical properties of f_h treated as a random variable (RV). The subscript n will be dropped since the derivations hold for any frequency index. In Section 3 the analysis is performed for the case of frequency instability spanning less than one DFT frequency bin Δf, *ie*, the case of low order harmonics typically characterized by low instability. In Section 4 the proposed approach is extended to the case where more than one DFT frequency bin is involved, *ie*, the case where higher order harmonics are considered.

3 STATISTICAL ANALYSIS: FREQUENCY INSTABILITY SPANNING ONE DFT BIN

If the frequency f of a sinusoidal component in the voltage waveform does not equal one of the DFT discrete frequencies (*ie*, the integer multiples of the frequency bin Δf), the related spectral-line magnitude does not take its ideal value. In fact, in this case (*ie*, the non-coherent sampling condition) the spectral line magnitude is weighted by the Fourier transform of the time window $w[k]$ used in (2) against spectral leakage. An approximate methodology is here introduced, consisting in the approximation of the frequency-domain behavior of each specific window by a parabolic function obtained by setting the constraint provided by the window Scallop Loss (SL) (see Fig. 1), *ie*, the maximum attenuation introduced by the window at the edges $\pm\Delta f/2$ of each DFT bin [13]. From Fig. 1, assuming the n-th DFT frequency bin as the origin of the frequency axis, the normalized weighted amplitude introduced by the window on a waveform spectral line can be readily obtained [4]:

$$y \cong 1 - \frac{4(1-SL)}{\Delta f^2} f^2 = 1 - 4(1-SL)x^2 \tag{3}$$

where $x = f/\Delta f$ is the normalized frequency.

Such attenuation is applied to the actual amplitude V of each sinusoidal component in (1). Therefore, the measured amplitude of each sinusoidal component can be written:

$$\hat{V} = yV \tag{4}$$

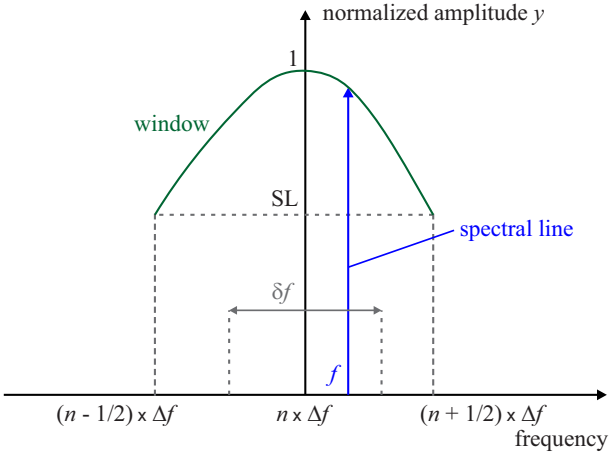

Fig. 1. Spectral line spanning less than one DFT bin, weighted by the frequency-domain window

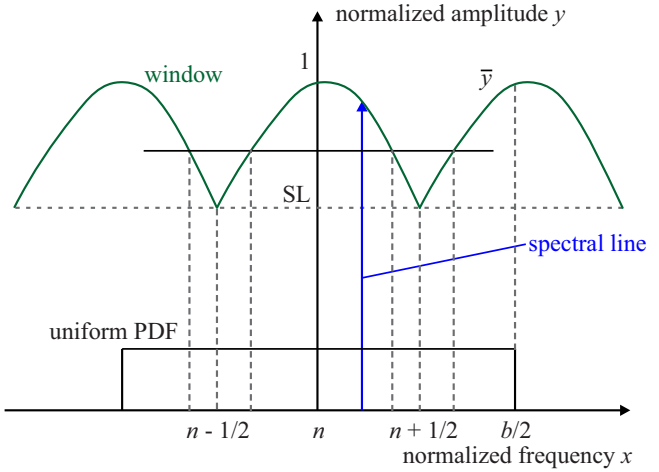

Fig. 2. Uniform distribution of a spectral line spanning more than one DFT bin

Table 1. Some figures of merit of three common windows

Window	NPSG	ENBW	SL (dB)	SL
Rect.	1	1	3.92	0.637
Tukey ($\alpha = 0.5$)	0.75	1.22	2.24	0.773
Hann	0.50	1.50	1.42	0.849

where V denotes the non-weighted frequency-centered spectral line.

In this Section the frequency f of the sine wave component is treated as a RV uniformly distributed within an interval δf centered on the DFT frequency bin $n \times \Delta f$ (see Fig. 1) and not exceeding Δf, *ie*, $\delta f \leq \Delta f$. Thus, the probability density function (PDF) of the spectral line frequency is $1/\delta f$ within the interval $\pm\delta f/2$. It follows that also y is a RV whose mean value and variance can be evaluated analytically in a straightforward way by taking into account (3) [14]

$$\mu_y = \int_{-\frac{1}{2}\delta f}^{\frac{1}{2}\delta f} y \frac{1}{\delta f} \mathrm{d}f = 1 - \frac{1}{3}(1 - SL)b^2, \tag{5}$$

$$\sigma_y^2 = \int_{-\frac{1}{2}\delta f}^{\frac{1}{2}\delta f} (y - \mu_y)^2 \frac{1}{\delta f} \mathrm{d}f = \frac{4}{45}(1 - SL)^2 b^4 \tag{6}$$

where

$$b = \frac{\delta f}{\Delta f} \tag{7}$$

is the normalized frequency instability.

The cumulative distribution function (CDF) of the RV y can be readily evaluated by considering that for a given value y the corresponding values of f can be obtained by inversion of (3) as

$$f_{1,2} = \pm\Delta f \sqrt{\frac{1 - y}{4(1 - SL)}}. \tag{8}$$

Therefore, by taking into account the frequency intervals defined by (8) and the uniformity of f, the CDF of the RV y can be derived as

$$P(y) = 1 - \frac{1}{b}\sqrt{\frac{1 - y}{1 - SL}}. \tag{9}$$

The PDF of the RV y can be readily obtained from (9) by derivation:

$$p(y) = \frac{\mathrm{d}P}{\mathrm{d}y} = \frac{1}{2b\sqrt{(1 - y)(1 - SL)}}. \tag{10}$$

Finally, by taking into account (4), the following analytical results hold for the measured harmonic amplitude [14]:

$$\mu_{\hat{V}} = \mu_y V, \tag{11}$$

$$\sigma_{\hat{V}} = \sigma_y^2 V^2, \tag{12}$$

$$P(\hat{V}) = 1 - \frac{1}{b}\sqrt{\frac{1 - (\hat{V}/V)}{1 - SL}}, \tag{13}$$

$$p(\hat{V}) = \frac{1}{V} \frac{1}{2b\sqrt{\big(1 - (\hat{V}/V)\big)\big(1 - SL\big)}}. \tag{14}$$

4 STATISTICAL ANALYSIS: FREQUENCY INSTABILITY INVOLVING MORE DFT BINS

In this Section the assumption of harmonic frequency ranging within only one DFT bin is removed. This can be the case of higher order harmonics characterized by wider frequency range of variability.

In Fig. 2 the case of a harmonic frequency with uniform distribution extending over the two DFT bins adjacent to the nominal bin is shown. The normalized frequency $x = f/\Delta f$ is here considered. The width of the normalized uniform distribution is $b = \delta f/\Delta f$, whereas the PDF

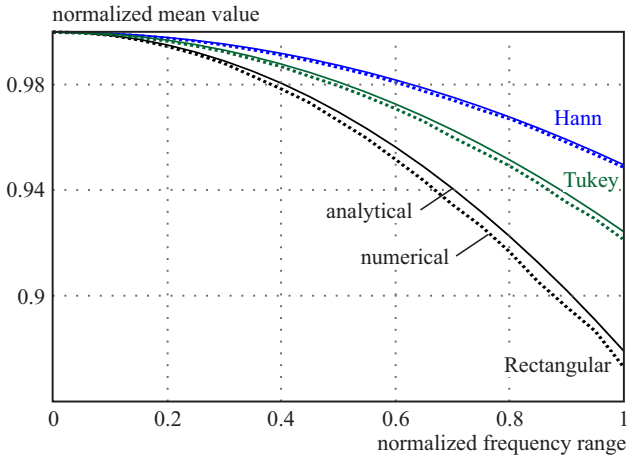

Fig. 3. Comparison between analytical (solid lines) and numerical (dotted lines) mean value of the amplitude of the fifth harmonic as a function of the normalized frequency range $\delta f/\Delta f$ due to frequency instability, for three different windows

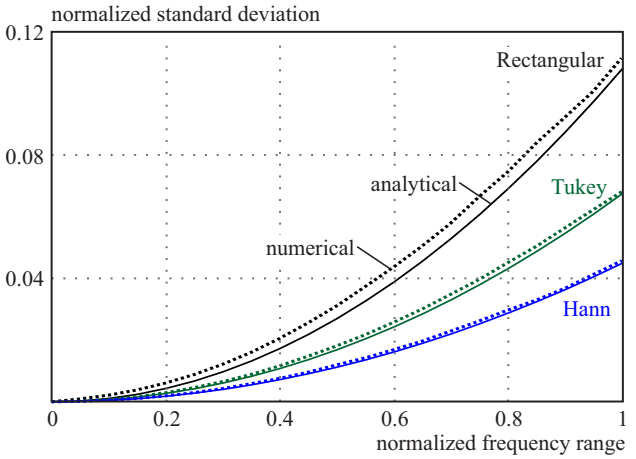

Fig. 4. Comparison between analytical (solid lines) and numerical (dotted lines) estimates of the normalized standard deviation of the amplitude of the fifth harmonic as a function of the normalized frequency range $\delta f/\Delta f$ due to frequency instability, for three different windows

magnitude is $1/b = \Delta f/\delta f$. The mean value and the variance of y can be evaluated similarly to (5) and (6) assuming $1 \le b \le 3$:

$$\mu_y = (1 - SL)\frac{(b-2)^3 + 2}{3b}\,, \tag{15}$$

$$\sigma_y^2 = \frac{(1-SL)^2}{b}\left\{\tfrac{1}{5}[(b-2)^5 + 2] - \tfrac{1}{9b}[(b-2)^3 + 2]^2\right\}. \tag{16}$$

The PDF of y in Fig. 2 can be readily obtained by resorting to the fundamental theorem of the PDF of a function of one random variable [14, 15]. Indeed the theorem requires the evaluation of the roots of $y = y(x)$, and the evaluation of the absolute value of the first derivatives of $y(x)$ in such roots. Notice that for a given y, all the related roots correspond to first derivatives with the same absolute value. From (3) we obtain that the first positive root is given by

$$x_1 = \sqrt{\frac{1-y}{4(1-SL)}} \tag{17}$$

and therefore all the first derivatives have absolute value

$$|y'(x_1)| = 4\sqrt{(1-SL)(1-y)}\,. \tag{18}$$

Thus, according to the fundamental theorem mentioned above, each root contributes to the PDF with the term

$$P_0(y) = \frac{1}{4b\sqrt{(1-SL)(1-y)}}\,. \tag{19}$$

The number of contributions (19) depends on the extension b of the frequency instability, and on the corresponding intervals defined for the variable y. By means of geometrical considerations based on Fig. 2, the following results can be derived.

For a frequency instability b such that $1 \le b \le 2$, the PDF of y is given by

$$p(y) = \begin{cases} 4p_0(y)\,, & SL \le y \le \overline{y}\,, \\ 2p_0(y)\,, & \overline{y} \le y \le 1 \end{cases} \tag{20}$$

where

$$\overline{y} = 1 - (1-SL)(b-2)^2. \tag{21}$$

For a frequency instability b such that $2 \le b \le 3$, the PDF of y is given by

$$p(y) = \begin{cases} 4p_0(y)\,, & SL \le y \le \overline{y}\,, \\ 6p_0(y)\,, & \overline{y} \le y \le 1 \end{cases} \tag{22}$$

where $\overline{y}$ is still given by (21).

Finally, the CDF can be readily obtained by direct integration of (20) and (22). The approach can be readily extended to the case of frequency instability spanning more than three DFT bins.

5 NUMERICAL VALIDATION

The analytical results derived in Sections 3 and 4 have been validated by resorting to numerical simulation of the whole digital measurement process. According to (1), a voltage waveform consisting of four harmonic components have been selected such that $f_1 = 50$ Hz, $f_3 = 3f_1$, $f_5 = 5f_1$, $f_{15} = 15f_1$. The voltage rms values have been selected as $V_1 = 10$, $V_3 = 2$, $V_5 = V_{15} = 1$. Phase angles have been selected at random. Sampling has been performed such that 10 nominal periods of the fundamental component are acquired, *ie*, a 200 ms measurement window was taken. The selection of the number of samples N_S defines the corresponding sampling frequency. By assuming $N_S = 2^{12}$ the corresponding sampling frequency is $f_S = 20.48$ kHz, and the related frequency resolution is

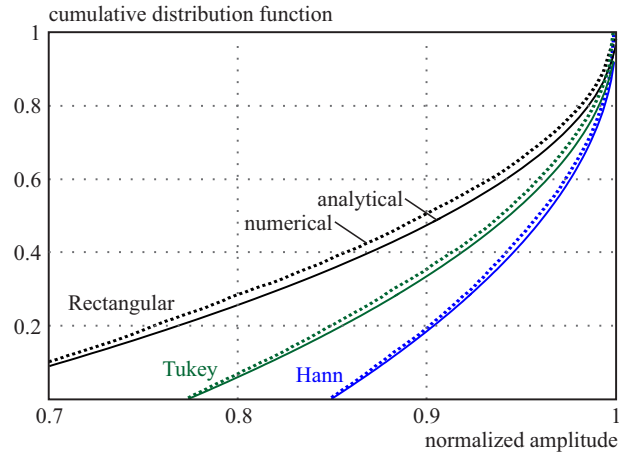

Fig. 5. Comparison between numerical and analytical CDF of the amplitude of the fifth harmonic under the assumption of normalized frequency range $\delta f/\Delta f = 1$, for three different windows

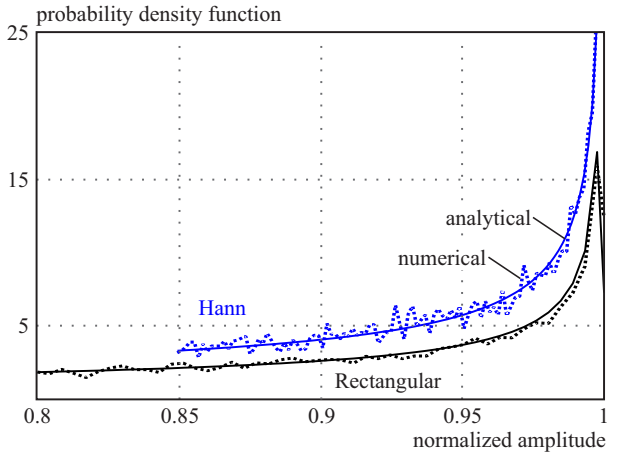

Fig. 6. Comparison between numerical and analytical PDF of the amplitude of the fifth harmonic under the assumption of normalized frequency range $\delta f/\Delta f = 1$, for two different windows

$\Delta f = 5$ Hz. A repeated run analysis (10^4 runs to estimate each average value) has been performed by assuming f_1 taking random values with uniform distribution within a frequency range δf centered on the nominal frequency 50 Hz. It is worth noticing that a frequency deviation δf in the fundamental component results in a frequency deviation $3\delta f$ in the third harmonic, $5\delta f$ in the fifth harmonic, and $15\delta f$ in the fifteenth harmonic. In the first set of the following simulations, analytical results (11)–(14) have been validated for the fifth harmonic. In fact, by assuming a maximum $\frac{\delta f}{\Delta f} = 0.2$ for the fundamental component, such normalized frequency range equals 1 for the fifth harmonic (*ie*, only one frequency bin as assumed in the derivations in Section 3).

In Fig. 3 the numerical estimates (dotted lines) of the mean value of the fifth harmonic amplitude are compared with the analytical result (11). The three different windows considered in Tab. 1 were used. Clearly the rectangular window shows the worst behavior due to its lowest SL value.

In Fig. 4 the numerical estimates (dotted lines) of the standard deviation of the fifth harmonic amplitude are compared with the analytical results (12) (*ie*, its square root). Also in this case the best behavior is provided by the Hann window due to its larger SL.

Figure 5 shows the behavior of the CDF of the amplitude of the fifth harmonic in the case of frequency instability involving the whole frequency bin, *ie*, $\delta f/\Delta f = 1$. Numerical results (dotted lines) and analytical results (solid lines) provided by (13) are in good agreement. The spread of the CDF is related to the SL of the window. Therefore, the rectangular window corresponds to a larger spread in the CDF.

Figure 6 shows the comparison between numerical and analytical PDF provided by (14) for the amplitude of the fifth harmonic under the same assumption as in Fig.5 for the frequency instability. In this case, for the sake of better graphical representation, the behavior corresponding to Tukey window is not shown (intermediate behavior between the other two cases). Similar remarks concerning the correlation between the SL magnitude and the PDF spread already mentioned above for the CDF can be provided.

A second set of simulations was performed to test the fifteenth harmonic. In this case the maximum frequency instability is 15 times the maximum frequency instability of the fundamental, *ie*, $15 \times \frac{\delta f}{\Delta f} = 3$. Therefore, the analytical results derived in Section 4 apply in this case, since frequency instability involves more than one DFT bin. Figure 7 shows the comparison between the analytical mean value provided by (15) (solid lines) and numerical results (dotted lines) for the three different windows already used in the previous simulations. Notice the oscillatory behavior due to the contribution of more than one DFT bin, in contrast with the monotonic behavior obtained in Fig. 3.

Figure 8 shows the behavior of the normalized standard deviation of the fifteenth harmonic amplitude as provided by the square root of (16) compared with numerical results. Also in this case the oscillatory behavior is in contrast with the monotonic behavior obtained in Fig. 4.

Figure 9 shows the PDF of the fifteenth harmonic amplitude for a relative frequency instability equal to 1.5. The relevant analytical result is given by (20). Notice that, according to (20), a discontinuous PDF is obtained in this case, where the discontinuity point was derived in (21). Moreover, notice that, according to (20), the PDF discontinuity consists in a negative step from $4p_0$ to $4p_0$. Finally, in Fig. 10 the PDFs are compared for the case of a relative frequency instability equal to 2.85. In this case the relevant analytical result is given by (22). In fact, notice that, in contrast with Fig. 9, in this case the PDF discontinuity consists in a positive step from $4p_0$ to $6p_0$.

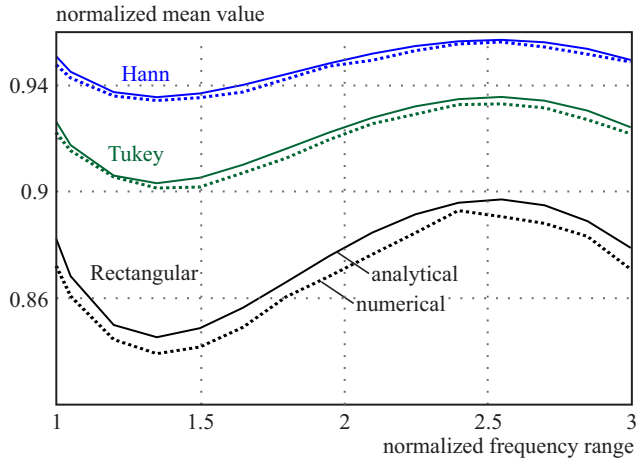

Fig. 7. Comparison between analytical (solid lines) and numerical (dotted lines) mean value of the amplitude of the fifteenth harmonic as a function of the normalized frequency range $\delta f/\Delta f$ due to frequency instability, for three different windows

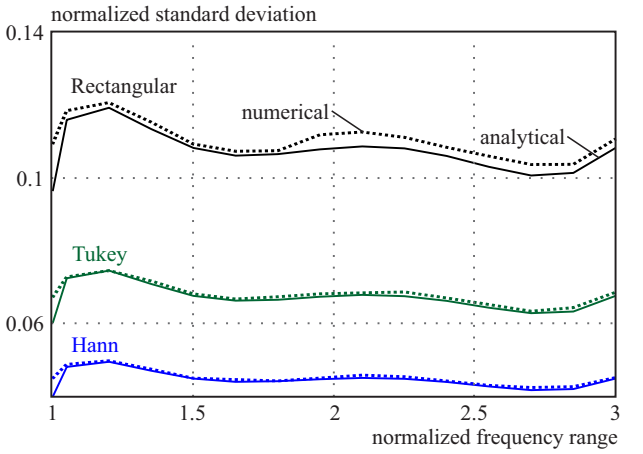

Fig. 8. Comparison between analytical (solid lines) and numerical (dotted lines) estimates of the normalized standard deviation of the amplitude of the fifteenth harmonic as a function of the normalized frequency range $\delta f/\Delta f$ due to frequency instability, for three different windows

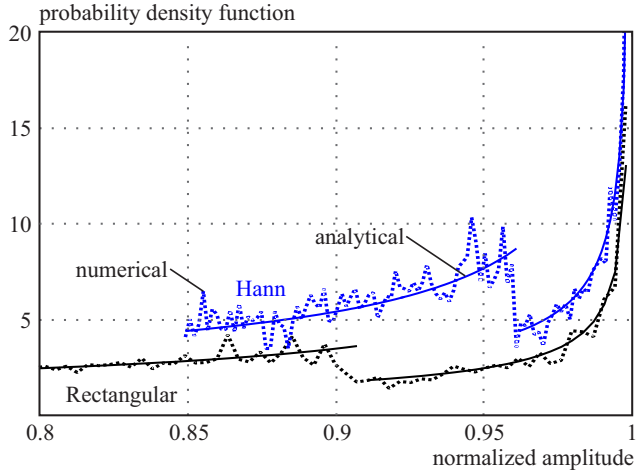

Fig. 9. Comparison between numerical and analytical PDF of the amplitude of the harmonic number 15 under the assumption of normalized frequency $\delta f/\Delta f = 1.5$, for two different windows

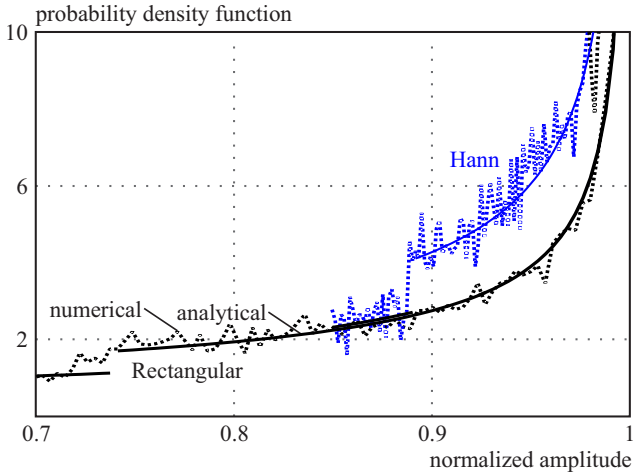

Fig. 10. Comparison between numerical and analytical PDF of the amplitude of the harmonic number 15 under the assumption of normalized frequency range $\delta f/\Delta f = 2.85$, for two different windows

6 CONCLUSION

An approximate analytical approach has been proposed in the paper to provide the statistical characterization of the DFT peaks magnitude corresponding to harmonics affected by frequency instability. The key point of the paper is the approximate representation of the frequency behavior of the window used in the time domain against spectral leakage, resulting in a weighting function for the harmonic spectral line. Such behavior has been approximated by a parabolic function having the window scallop loss as parameter. By modeling the frequency of each harmonic as a random variable with uniform distribution, the mean value, the standard deviation, the CDF and the PDF of the corresponding DFT peak have been derived in analytical form. The advantage of the proposed approach is its simplicity and the possibility to be used in a straightforward way for a general window by using only the scallop loss of the selected window as parameter. In fact, numerical simulations corresponding to three windows characterized by different values of the scallop loss have shown very good agreement with analytical results.

Future work will be devoted to include in the model more general statistical distributions of the frequency instability such as unbounded and possibly non-symmetrical distributions (*ie*, the case of inter-harmonic components).

References

[1] BELLAN, D.—SPADACINI, G,—FEDELI, E.——PIGNARI, S. A.: Space-Frequency Analysis and Experimental Measurement of Magnetic Field Emissions Radiated by High-Speed Rail-

way Systems, IEEE Trans. Electromagn. Compat. **55** No. 6 (2013), 1031–1042.

[2] LIN, T.—DOMIJAN, A.: On Power Quality Indices and Real Time Measurement, IEEE Trans. on Power Delivery **20** No. 4 (2005), 2552–2562.

[3] VEDADY MOGHADAM, M. R.—MA, R. T. B.—ZHANG, R.: Distributed Frequency Control in Smart Grids via Randomized Demand Response, IEEE Trans. on Smart Grid **5** No. 6 (2014), 2798–2809.

[4] BELLAN, D.: Frequency Instability and Additive Noise Effects on Digital Power Measurements under Non-Sinusoidal Conditions, In: 2014 6th IEEE Power India International Conference (PIICON), 2014, pp. 1–5.

[5] WANG, M. H.—SUN, Y. Z.: A Practical, Precise Method for Frequency Tracking and Phasor Estimation, IEEE Trans. on Power Delivery **19** No. 4 (2004), 1547–1552.

[6] BELEGA, D.—DALLET, D.—PETRI, D.: Accuracy of Sine Wave Frequency Estimation by Multipoint Interpolated DFT Approach, IEEE Trans. on Instrum. Meas. **59** No. 11 (2010), 2808–2815.

[7] WANG, M.—SUN, Y.: A Practical Method to Improve Phasor and Power Measurement Accuracy of DFT Algorithm, IEEE Trans. on Power Delivery **21** No. 3 (2006), 1054–1062.

[8] SOLOMON, O. M.: The Use of DFT Windows in Signal-to-Noise Ratio and Harmonic Distortion Computations, IEEE Trans. Instrum. Meas. **43** No. 2 (1994), 194–199.

[9] BELLAN, D.: Statistical Characterization of Harmonic Emissions in Power Supply Systems, International Review of Electrical Engineering **9** No. 4 (2014), 803–810.

[10] BELLAN, D.: Characteristic Function of Fundamental and Harmonic Active Power in Digital Measurements under Non-sinusoidal Conditions, International Review of Electrical Engineering **10** No. 4 (2015), 520–527.

[11] BELLAN, D.: Noise Propagation in Multiple-Input ADC-based Measurement Systems, Measurement Science Review **14** No. 6 (2014), 302–307.

[12] BELLAN, D.: On the Validity of the Noise Model of Quantization for the Frequency-Domain Amplitude Estimation of Low-Level Sine Waves, Metrology and Measurement Systems **22** No. 1 (2015), 89–100.

[13] HARRIS, F. J.: On the Use of Windows for Harmonic Analysis with the Discrete Fourier Transform, Proc. of the IEEE **66** (1978), 51–83.

[14] PAPOULIS—PILLAI, S. U.: Probability, Random Variables and Stochastic Processes, McGraw-Hill, 4th Ed., 2002.

[15] BELLAN, D.—PIGNARI, S. A.: Statistical Superposition of Crosstalk Effects in Cable Bundles, China Communications **10** No. 11 (2013), 119–128.

Received 5 March 2016

Diego Bellan is an Assistant Professor of Circuit Theory at the Politecnico di Milano, where he is currently with the Department of Electronics, Information and Bioengineering. His research interests are in the field of Electromagnetic Compatibility (EMC) and analog-to-digital conversion of signals, and include field-to-wire coupling and crosstalk in multiwire structures, EMC in railway systems, and statistical signal processing.

Sergio A. Pignari joined Politecnico di Milano, Milan, Italy, in 1998, where he is currently a Full Professor of Circuit Theory and Electromagnetic Compatibility (EMC) with the Department of Electronics, Information and Bioengineering. His research interests are in the field of EMC and include field-to-wire coupling and crosstalk in multiwire structures, statistical techniques for EMC, experimental procedures and setups for EMC testing. He is currently an Associate Editor of the IEEE Trans. on Electromagnetic Compatibility.